

Thermoelectric properties of Al-doped $\text{Mg}_2\text{Si}_{1-x}\text{Sn}_x$ ($x \leq 0.1$)

Jun-ichi Tani*, Hiroyasu Kido

Department of Electronic Materials, Osaka Municipal Technical Research Institute,
1-6-50 Morinomiya, Joto-ku, Osaka 536-8553, Japan

Received 14 August 2007; accepted 11 November 2007

Available online 19 November 2007

Abstract

The thermoelectric properties of Al-doped $\text{Mg}_2\text{Si}_{1-x}\text{Sn}_x$ ($x=0.0-0.1$) [$\text{Mg}_2\text{Si}_{1-x}\text{Sn}_x:\text{Al}=1:y$ ($0.00 \leq y \leq 0.02$)] fabricated by spark plasma sintering have been characterized by Hall effect measurements at 300 K and by measurements of electrical resistivity (ρ), the Seebeck coefficient (S), and thermal conductivity (κ) between 300 and 900 K. Al-doped $\text{Mg}_2\text{Si}_{1-x}\text{Sn}_x$ samples are n-type in the measured temperature range. By Al-doping, electron concentration is controlled up to $5.3 \times 10^{19} \text{ cm}^{-3}$ in the composition range $0.0 \leq x \leq 0.1$. Al-doped $\text{Mg}_2\text{Si}_{0.9}\text{Sn}_{0.1}$ shows a maximum value of the figure of merit ZT of 0.68 at 864 K, which is 6 times larger than that of nondoped $\text{Mg}_2\text{Si}_{0.9}\text{Sn}_{0.1}$.

© 2007 Elsevier B.V. All rights reserved.

Keywords: Intermetallics; Thermoelectric materials; Electrical transport; Impurities in semiconductors

1. Introduction

Mg_2X ($\text{X}=\text{Si}$, Ge , and Sn) and their solid solutions have been considered as candidates for high-performance thermoelectric materials [1–11]. For thermoelectric materials, a large Seebeck coefficient, S , a small electrical resistivity, ρ , and a small thermal conductivity, κ , are required. These quantities determine the thermoelectric figure of merit, $Z=S^2/\rho\kappa$. A low lattice thermal conductivity and high carrier mobility are desirable for improvement of the figure of merit. Vining [12] pointed out that the factor $A'=(T/300)(m^*/m_e)^{3/2}\mu/\kappa_{\text{ph}}$, where m^* is the carrier effective mass, μ is the mobility in $\text{cm}^2/(\text{V s})$, and κ_{ph} is the lattice thermal conductivity in $\text{mW}/(\text{cm K})$, has a larger value of 3.7–14 for Mg_2X , when compared with 1.2–2.6 for SiGe and 0.05–0.8 for $\beta\text{-FeSi}_2$, and therefore, a Mg_2X system will achieve a higher ZT with further development. In the solid solutions of $\text{Mg}_2\text{Si}_{1-x}\text{Ge}_x$, $\text{Mg}_2\text{Si}_{1-x}\text{Sn}_x$, and $\text{Mg}_2\text{Ge}_{1-x}\text{Sn}_x$, it is pointed out that the lowest lattice thermal conductivity can be achieved in the system $\text{Mg}_2\text{Si}_{1-x}\text{Sn}_x$ due to the maximum atomic mass difference between the components [13]. Recently, Zaitsev et al. [5] reported the thermoelectric properties of Sb-doped $\text{Mg}_2\text{Si}_{1-x}\text{Sn}_x$ ($x=0.4$ and 0.6), and the maximum value of ZT reaches 1.1, which exceeds the unity. Therefore, impurity-

doped $\text{Mg}_2\text{Si}_{1-x}\text{Sn}_x$ is a promising thermoelectric material for cheap, ecologically friendly, light, and high-performance thermoelectric generators in the middle temperature range.

Kajikawa et al. [14] and Umemoto et al. [9] reported the thermoelectric properties of Mg_2Si fabricated by spark plasma sintering (SPS), which is a novel process because it is reported that the diffusion velocity becomes extremely large even at low temperatures owing to the pulse dc electric field. In the case of Mg_2Si , SPS plays two roles: (a) a solid-state reaction process between Mg and Si; (b) a densification process in a short time at relatively low temperatures, which is effective in suppressing the volatilization of Mg as well as dopants with low melting point. Al is expected to be one of the attractive dopants because of its cheap and nontoxic element. Umemoto et al. [9] reported that ZT of Al-doped Mg_2Si shows 0.57 at 856 K. However, to our knowledge, there have been no reports concerning the effect of Sn substitution on the thermoelectric properties of Al-doped Mg_2Si . A small amount of Sn substitution will affect the transport and thermoelectric properties of Al-doped Mg_2Si .

In the present study, we have fabricated Al-doped $\text{Mg}_2\text{Si}_{1-x}\text{Sn}_x$ ($x \leq 0.1$) by the SPS method, and the transport and thermoelectric properties have been characterized by Hall effect measurements at 300 K and by measurements of electrical resistivity, the Seebeck coefficient, and thermal conductivity between 300 and 900 K.

* Corresponding author.

E-mail address: tani@omtri.city.osaka.jp (J.-i. Tani).

2. Experimental method and details of the calculations

Powders of high purity, Mg (>99.9%), Si (>99.999%), Sn (>99.9%), and Al (>99.9%), were used as starting materials. Constituent Mg, Si, Sn, and Al powders were ground together and then heated at 993–1053 K for 10 min at 20 MPa in a graphite die (15 mm in diameter) in vacuum (<4 Pa) by the SPS method with a heating rate of 30–50 K/min. The density of the annealed samples was more than 99% of the theoretical value. X-ray diffraction of the samples by Cu K α radiation detected only the antifluorite structure. The Hall coefficient (R_H) was measured for 1.5-cm-diameter, 0.1-cm-thick samples using the Toyo Corp. Resitest 8320. Contacts between the samples and lead Au wires were formed by soldering with indium. The Hall effect was measured at 300 K using an ac magnetic method under an applied magnetic field of 0.39 T at a frequency of 200 mHz. The carrier concentration (n) of the samples was determined by the factor $1/e|R_H|$. The error for the Hall coefficient was estimated to be less than $\pm 7\%$. The Seebeck coefficient (S) was measured by the standard technique using Pt electrodes in a He gas atmosphere in the temperature range of 300–900 K using an ULVAC ZEM-1S. The temperature gradient across the length of the sample was about 5 K. The error of the Seebeck coefficient measurements was estimated to be less than $\pm 5\%$. The electrical resistivity (ρ) was also measured concurrently by the four-probe dc method. The error of the electrical resistivity measurements was estimated to be less than $\pm 5\%$. The thermal diffusion coefficients of the samples were measured by the conventional laser flash method using a thermal constant analyzer (ULVAC TC-7000). The disk specimen was set in an electric furnace and heated to 900 K under vacuum. After the temperature was stabilized, the front surface of the specimen was irradiated by a ruby laser pulse. The temperature variation at the surface was monitored using a Pt–Pt 13% Rh thermocouple and an InSb infrared detector. The error of the thermal diffusion coefficients measurements was estimated to be less than $\pm 5\%$. The density was measured by the Archimedes method. The thermal conductivity (κ) was calculated from the experimental thermal diffusivity (α), density (d), molecular weight (M_w) calculated from the chemical formula ($Mg_2Si_{1-x}Sn_x$), and a previously reported molar specific heat capacity (C_p) for nondoped Mg_2Si [15]. κ is given by the following Eq. (1):

$$\kappa = \frac{\alpha \times d \times C_p}{M_w} \quad (1)$$

To investigate the electronic and geometrical structure of Al-doped Mg_2Si , density functional theory (DFT) calculations within the pseudopotential and generalized gradient approximations (GGAs) were performed using the computer program CASTEP (Cambridge Serial Total Energy Package in Material Modeling, Accelrys) [16]. We constructed a supercell containing 48 atoms ($Mg_{32}Si_{16}$) with the space group $Fm\bar{3}m$ and replaced one of the 48 sites of the Mg or Si atoms by Al. We expanded the valence electronic wave functions in a plane-wave basis set up to an energy cutoff of 400 eV, which converges the total energy of the unit cell to better than 1 meV/atom. In the total energy calculations, integrations over the Brillouin zone were performed using a $3 \times 2 \times 2$ Monkhorst-Pack set [17], which gives six symmetrized k points in the irreducible Brillouin zone for the 48-atom unit cell. The electron–ion interaction is described using Vanderbilt’s ultrasoft pseudopotentials [18]. The lattice constant was determined through calculations for the primitive cell, using a plane-wave cutoff energy of 400 eV;

the calculated value is 99.9% of the experimental value reported for Mg_2Si [19]. The positions of the atoms within the second-nearest neighbors of the impurity were allowed to relax under a constant volume condition by total energy minimization, until the residual forces for the relaxed atoms were <0.1 eV/Å.

3. Results and discussion

Table 1 lists the transport properties of Al-doped $Mg_2Si_{1-x}Sn_x$ ($x=0.0-0.1$) at 300 K, compared with those of $Mg_2Si_{1-x}Sn_x$ without Al-doping. R_H for Al-doped $Mg_2Si_{1-x}Sn_x$ is negative, indicating that the conductivity is mainly due to electrons. The Hall mobility ($\mu_H = R_H/\rho$) at 300 K of Al-doped Mg_2Si (163 cm 2 /(V s)) is lower than the value for nondoped Mg_2Si (204 cm 2 /(V s)). μ_H of Al-doped or nondoped $Mg_2Si_{1-x}Sn_x$ ($x=0.05-0.1$) shows $101-116$ cm 2 /(V s), which is lower than that of Al-doped or nondoped Mg_2Si . The carrier concentration of $Mg_2Si_{1-x}Sn_x$ without Al-doping is from 4.3×10^{17} cm $^{-3}$ for $x=0.0$ to 3.7×10^{18} cm $^{-3}$ for $x=0.05$, while that of Al-doped $Mg_2Si_{1-x}Sn_x$ [$Mg_2Si_{1-x}Sn_x:Al=1:y$ ($0.005 \leq y \leq 0.02$)] is from 2.0×10^{19} cm $^{-3}$ for $y=0.0005$ to 5.3×10^{19} cm $^{-3}$ for $y=0.02$. The carrier concentration of Al-doped $Mg_2Si_{1-x}Sn_x$ is controlled up to 5.3×10^{19} cm $^{-3}$ by Al-doping, but x does not affect the maximum carrier concentration.

Fig. 1 shows the temperature dependence of the electrical resistivity (ρ) of Al-doped $Mg_2Si_{1-x}Sn_x$ ($x=0.0-0.1$), compared with those of $Mg_2Si_{1-x}Sn_x$ without Al-doping. ρ for Al-doped $Mg_2Si_{1-x}Sn_x$ ($x=0.0-0.1$) as well as $Mg_2Si_{1-x}Sn_x$ without Al-doping increases, reaching a maximum at 470–670 K, and then decreases or shows a constant with increasing temperature. LaBotz et al. [1] and Noda et al. [4] reported that the temperature dependence of mobility in $Mg_2Si_xGe_{1-x}$ indicates that $\mu \propto T^{-3/2}$ and that acoustic lattice scattering is the predominant mechanism. Therefore, the increase in ρ at low temperatures is explained by the decrease in mobility with increasing temperature. The decrease in ρ at high temperatures is explained by the fact that intrinsic conduction occurs because of the band gap of ~ 0.7 eV [20–22].

Although the experimental results showing the n-type conduction of Al-doped Mg_2Si suggest that Al atoms (IIIb group) are primarily located at the Mg sites (IIa group) in Mg_2Si and that Al atoms act as donors. However, Imai et al. [23] reported that it is energetically favorable that doped Al atoms in Mg_2Si would substitute Si atoms rather than Mg atoms from first-principles

Table 1
Transport properties of Al-doped $Mg_2Si_{1-x}Sn_x$ ($x=0.0-0.1$) [$Mg_2Si_{1-x}Sn_x:Al=1:y$ ($0.005 \leq y \leq 0.02$)], compared with those of $Mg_2Si_{1-x}Sn_x$ without Al-doping at 300 K

Sample number	Sn (x)	Al (y)	Carrier type	Carrier concentration (cm $^{-3}$)	Mobility [cm 2 /(V s)]	Resistivity (Ω cm)
#1	0.00	0.000	N	4.3×10^{17}	204	7.14×10^{-2}
#2	0.05	0.000	N	3.7×10^{18}	107	1.57×10^{-2}
#3	0.10	0.000	N	2.9×10^{18}	106	2.02×10^{-2}
#4	0.00	0.005	N	5.3×10^{19}	163	7.18×10^{-4}
#5	0.05	0.005	N	3.6×10^{19}	116	1.50×10^{-3}
#6	0.05	0.020	N	5.3×10^{19}	105	1.14×10^{-3}
#7	0.10	0.005	N	2.0×10^{19}	114	2.73×10^{-3}
#8	0.10	0.010	N	4.6×10^{19}	112	1.21×10^{-3}
#9	0.10	0.020	N	5.3×10^{19}	101	1.17×10^{-3}

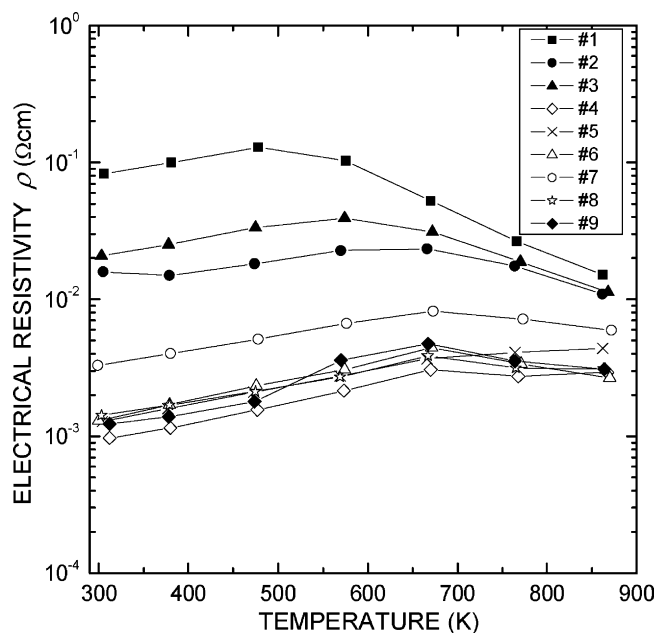


Fig. 1. Electrical resistivity (ρ) of Al-doped $\text{Mg}_2\text{Si}_{1-x}\text{Sn}_x$ ($x=0.0-0.1$), compared with those of $\text{Mg}_2\text{Si}_{1-x}\text{Sn}_x$ without Al-doping.

calculations based on unrelaxed structure. This result might be caused by insufficient treatment of lattice relaxation. Thus, we performed quantum-mechanical first-principles calculations of Al-doped Mg_2Si based on the relaxed structure. The formation energies of impurities in the neutral charge state are [24–26]

$$E_{\text{formation}} = E_{\text{T}} - n_{\text{Mg}}\mu_{\text{Mg}} - n_{\text{Si}}\mu_{\text{Si}} - \mu_{\text{Al}} \quad (2)$$

where E_{T} is the total energy of a supercell containing an Al atom ($\text{Mg}_{31}\text{AlSi}_{16}$ or $\text{Mg}_{32}\text{Si}_{15}\text{Al}$); n_{Mg} and n_{Si} represent the number of Mg and Si atoms, respectively, in the supercell; μ_{Mg} , μ_{Si} , and μ_{Al} are the chemical potentials of Mg, Si, and Al atoms, respectively.

The chemical potentials of μ_{Mg} and μ_{Si} can be varied within a range limited by the three constraints:

$$\mu_{\text{Mg}} \leq \mu_{\text{Mg}(\text{bulk})}, \quad (3)$$

$$\mu_{\text{Si}} \leq \mu_{\text{Si}(\text{bulk})}, \quad (4)$$

$$2\mu_{\text{Mg}} + \mu_{\text{Si}} = \mu_{\text{Mg}_2\text{Si}(\text{bulk})}, \quad (5)$$

where $\mu_{\text{Mg}_2\text{Si}(\text{bulk})}$, the chemical potential of the bulk Mg_2Si , is a constant value calculated as the total energy per Mg_2Si unit formula. $\mu_{\text{Mg}(\text{bulk})}$ and $\mu_{\text{Si}(\text{bulk})}$ are calculated as the total energies per a Si atom from the Si crystal (space group: $Fd\bar{3}m$, cubic structure), and a Mg atom from the Mg crystal (space group: $P6_3/mmc$, hexagonal structure), respectively.

The formation energies were calculated under two extreme conditions: the Si-rich limit ($\mu_{\text{Mg}} = 1/2(\mu_{\text{Mg}_2\text{Si}(\text{bulk})} - \mu_{\text{Si}(\text{bulk})})$ and $\mu_{\text{Si}} = \mu_{\text{Si}(\text{bulk})}$) and the Mg-rich limit ($\mu_{\text{Si}} = \mu_{\text{Mg}_2\text{Si}(\text{bulk})} - 2\mu_{\text{Mg}(\text{bulk})}$ and $\mu_{\text{Mg}} = \mu_{\text{Mg}(\text{bulk})}$). At the solubility limit that Al-doped Mg_2Si is equilibrium with Al metal or Al-Mg compound, μ_{Al} is determined using the total energies of Al crystal (space group: $Fm\bar{3}m$, cubic structure) and of two Al-Mg compounds [$\text{Al}_{12}\text{Mg}_{17}$ (space group: $I\bar{4}3m$, cubic structure)

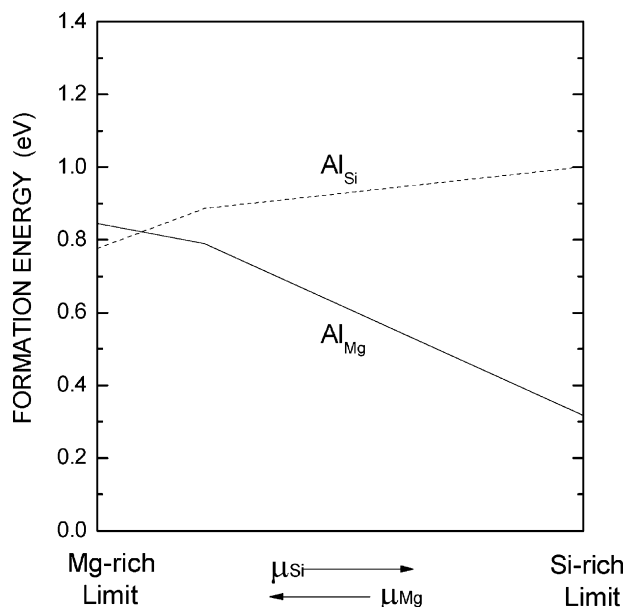


Fig. 2. Formation energy of Al as a dopant in Mg_2Si at the solubility limit. Subscripts indicate the sites of Al.

and $\text{Al}_{30}\text{Mg}_{23}$ (space group: $R\bar{3}H$, trigonal structure)], which are calculated after optimization of the structure.

Fig. 2 shows the formation energy of Al in Mg_2Si at the solubility limit. The formation energy of Si-site substitution is 0.78 and 1.00 eV at the Mg- and Si-rich limits, respectively. On the other hand, the formation energy of Mg-site substitution is 0.85 and 0.32 eV at the Mg- and Si-rich limits, respectively. At the Mg-rich limit, the formation energy of Mg-site substitution is as same as that of Si-site substitution. However, at the condition except Mg-rich limit, the substitution at the Mg sites is energetically lower than that at the Si sites. At the Si-rich limit, the formation energy of Mg-site substitution is 0.68 eV lower than that of Si-site substitution. Our calculations predict that Al atoms are primarily located at the Mg sites in Mg_2Si , at the condition except Mg-rich limit. The calculation result is in good agreement with the experimental results, showing n-type conduction, on the Hall effect as well as the Seebeck coefficient.

Fig. 3 shows the temperature dependence of the Seebeck coefficient (S) of Al-doped $\text{Mg}_2\text{Si}_{1-x}\text{Sn}_x$ ($x=0.0-0.1$), compared with those of $\text{Mg}_2\text{Si}_{1-x}\text{Sn}_x$ without Al-doping. The polarity of S for Al-doped Mg_2Si is negative, indicating that the conductivity is mainly due to electrons. The polarity of S is in good agreement with the sign of R_{H} at 300 K. The absolute value of S at ~ 310 K corresponds to the increase in electron concentration. The temperature at which $|S|$ shows a maximum is ~ 470 K for $\text{Mg}_2\text{Si}_{1-x}\text{Sn}_x$ without Al-doping, ~ 670 K for Al-doped $\text{Mg}_2\text{Si}_{1-x}\text{Sn}_x$ ($x=0.0-0.1$).

Fig. 4 shows the electron concentration dependence of the Seebeck coefficient at 300 K of Al-doped $\text{Mg}_2\text{Si}_{1-x}\text{Sn}_x$ ($x=0.0-0.1$). S at 300 K was estimated for each sample by the linear extrapolation of $S(T)$ between ~ 310 K and ~ 380 K to $T=300$ K. The Seebeck coefficient depends strongly on the electron concentration (n) in Al-doped $\text{Mg}_2\text{Si}_{1-x}\text{Sn}_x$ ($x=0.0-0.1$). The Seebeck coefficient is expressed theoretically in terms of

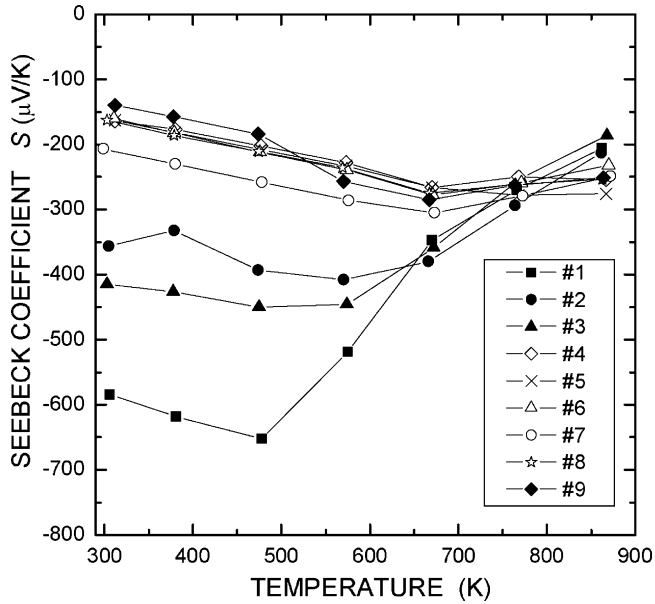


Fig. 3. Seebeck coefficient (S) of Al-doped $\text{Mg}_2\text{Si}_{1-x}\text{Sn}_x$ ($x=0.0-0.1$), compared with those of $\text{Mg}_2\text{Si}_{1-x}\text{Sn}_x$ without Al-doping.

Fermi–Dirac statistics. For a single-band model, S and n are given by [27]

$$S = \pm \frac{k_B}{e} \left(\frac{(2+r)F_{1+r}(\eta^*)}{(1+r)F_r(\eta^*)} - \eta^* \right), \quad (6)$$

$$n = 4\pi \left(\frac{2m^* k_B T}{h^2} \right)^{3/2} F_{1/2}(\eta^*), \quad (7)$$

where η^* is the reduced Fermi level ($=E_F/k_B T$, E_F is the Fermi level), e is the elementary charge, m^* is the carrier effective mass, T is the absolute temperature, and k_B and h are Boltzmann's and Planck's constants, respectively. The + and – signs

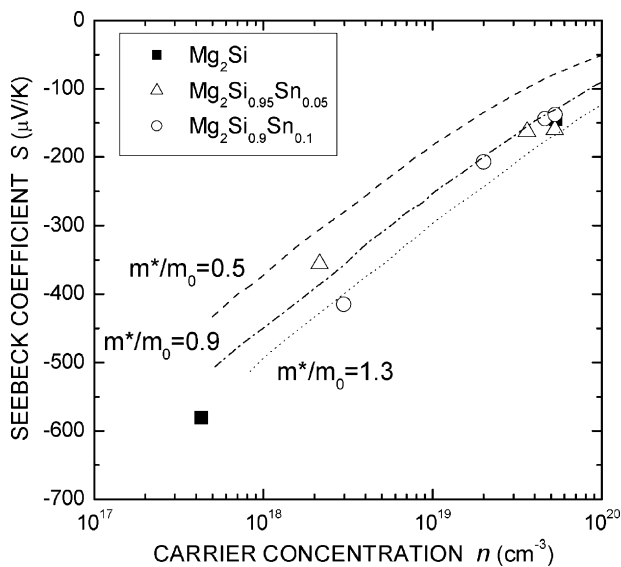


Fig. 4. Seebeck coefficient (S) at 300 K of Al-doped $\text{Mg}_2\text{Si}_{1-x}\text{Sn}_x$ ($x=0.0-0.1$) and $\text{Mg}_2\text{Si}_{1-x}\text{Sn}_x$ without Al-doping as a function of electron concentration (n). The dashed curve, dash-dotted curve, and dotted curve were calculated from Eq. (6) with $r=0.0$ and $m^*/m_0=0.5, 0.9$, or 1.3 , respectively.

in Eq. (6) refer to the contributions from holes and electrons, respectively. The scattering parameter r gives the exponent of the energy dependence of the charge carrier mean free path. When the carrier scattering is by acoustic phonons and ionized impurities, r takes the values of 0 and 2, respectively. The Fermi–Dirac integrals $F_r(\eta^*)$ for integral and half-integral orders have been tabulated in some studies [28–31]. In n-type Mg_2Si , r is estimated to be 0.0 from the temperature dependence of the Hall mobility corresponding to the acoustic phonon scattering [1,3]. Using $r=0.0$, our experimental data for the Seebeck coefficient at 300 K for n-type Al-doped $\text{Mg}_2\text{Si}_{1-x}\text{Sn}_x$ were found to be in good agreement with the calculation curves using $m^*/m_0=1.1 \pm 0.2$. The value of m^*/m_0 is consistent with previous results, $m^*/m_0=1.0$ reported for n-type nondoped Mg_2Si [1], $m^*/m_0=1.1 \pm 0.2$ reported for n-type P-doped Mg_2Si [11], and $m^*/m_0=1.2 \pm 0.2$ reported for n-type Sb-doped $\text{Mg}_2\text{Si}_{0.6}\text{Ge}_{0.4}$ [3].

Fig. 5 shows the temperature dependence of thermal conductivity (κ) of Al-doped $\text{Mg}_2\text{Si}_{1-x}\text{Sn}_x$ ($x=0.0-0.1$), compared with those of $\text{Mg}_2\text{Si}_{1-x}\text{Sn}_x$ without Al-doping. κ of $\text{Mg}_2\text{Si}_{1-x}\text{Sn}_x$ depends strongly on the amount of Sn substitution. κ of $\text{Mg}_2\text{Si}_{1-x}\text{Sn}_x$ is also influenced by the Al-doping in the high temperature range. κ is the sum of the contributions from the lattice (κ_{ph}) and electronic (κ_{el}) components. To understand the thermal conductivity behavior of Al-doped $\text{Mg}_2\text{Si}_{1-x}\text{Sn}_x$, it is necessary to determine the temperature and composition dependences of κ_{ph} and κ_{el} . We can calculate κ_{el} using the Wiedemann–Franz law [32], $\kappa_{\text{el}}=L_0\sigma T$ (L_0 : Lorentz number $2.45 \times 10^{-8} \text{ V}^2/\text{K}^2$, σ : electrical conductivity, T : absolute temperature). It is possible to calculate κ_{ph} by subtracting κ_{el} from κ .

Fig. 6 shows the temperature dependence of κ_{ph} and κ_{el} in the thermal conductivity of Al-doped $\text{Mg}_2\text{Si}_{1-x}\text{Sn}_x$ ($x=0.0-0.1$), compared with those of $\text{Mg}_2\text{Si}_{1-x}\text{Sn}_x$ without Al-doping.

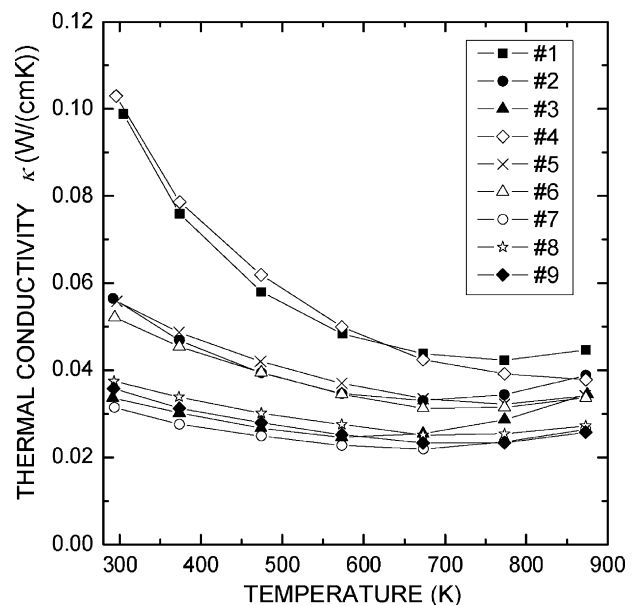


Fig. 5. Thermal conductivity (κ) of Al-doped $\text{Mg}_2\text{Si}_{1-x}\text{Sn}_x$ ($x=0.0-0.1$), compared with those of $\text{Mg}_2\text{Si}_{1-x}\text{Sn}_x$ without Al-doping.

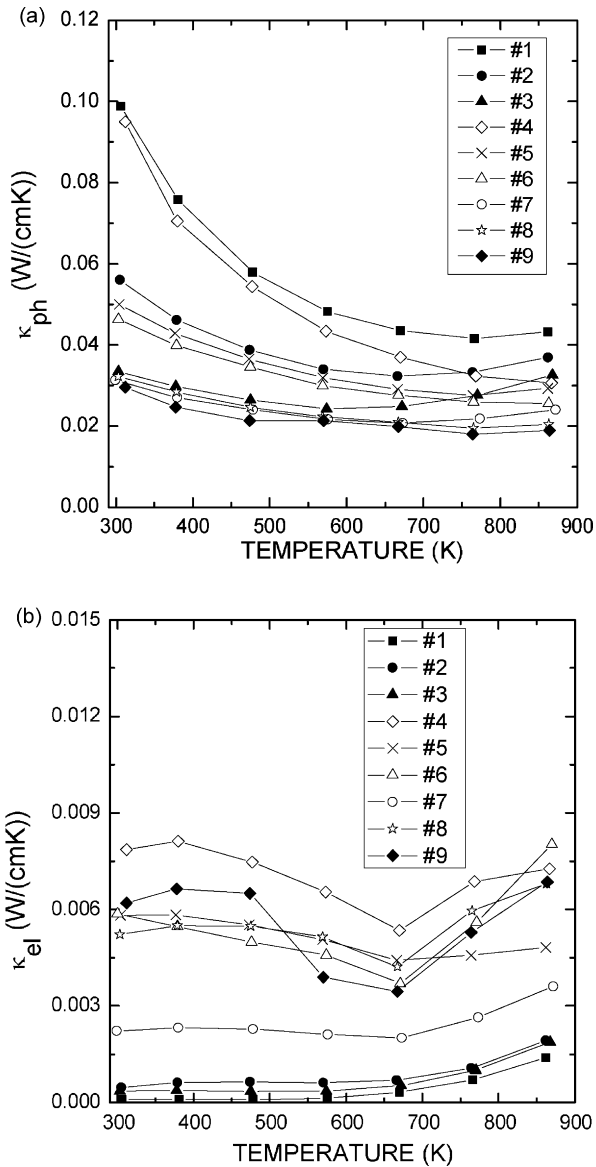


Fig. 6. (a) Lattice contribution (κ_{ph}) and (b) carrier contribution (κ_{el}) in the thermal conductivity of Al-doped $Mg_2Si_{1-x}Sn_x$ ($x=0.0-0.1$), compared with those of $Mg_2Si_{1-x}Sn_x$ without Al-doping.

κ_{ph} at low temperatures depends strongly on x . However, κ_{ph} at high temperatures depends on Al-doping concentration as well as x . κ_{ph} at ~ 300 K for nondoped Mg_2Si is 0.099 W/(cm K), which is consistent with that of Al-doped Mg_2Si (0.095 W/(cm K)). However, κ_{ph} at ~ 865 K for nondoped Mg_2Si is 0.043 W/(cm K) is 39% higher than that of Al-doped Mg_2Si (0.031 W/(cm K)). On the other hand, κ_{ph} at ~ 300 K for nondoped $Mg_2Si_{0.9}Sn_{0.1}$ is 0.033 W/(cm K), which is consistent with that of Al-doped $Mg_2Si_{0.9}Sn_{0.1}$ ($0.030-0.032$ W/(cm K) for $y=0.005-0.02$). However, κ_{ph} at ~ 865 K for nondoped $Mg_2Si_{0.9}Sn_{0.1}$ is 0.033 W/(cm K), which is 74% higher than that of Al-doped $Mg_2Si_{0.9}Sn_{0.1}$ (0.019 W/(cm K) for $y=0.02$). κ_{el} depends strongly on the Al-doping concentration. κ_{el} of Al-doped $Mg_2Si_{1-x}Sn_x$ ($x=0.0-0.1$) is much higher than that of $Mg_2Si_{1-x}Sn_x$ without Al-doping. κ_{el} of Al-doped Mg_2Si is the highest value because of the lowest electrical resistivity. The

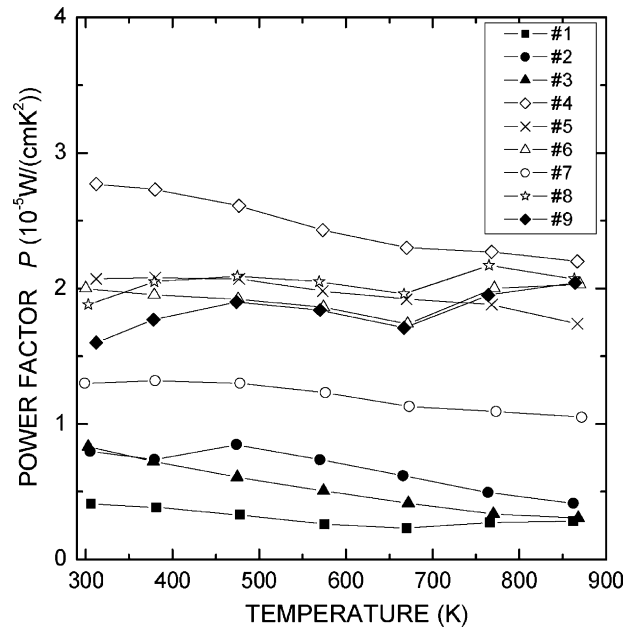


Fig. 7. Power factor (P) of Al-doped $Mg_2Si_{1-x}Sn_x$ ($x=0.0-0.1$), compared with those of $Mg_2Si_{1-x}Sn_x$ without Al-doping.

thermal conductivity of Al-doped $Mg_2Si_{1-x}Sn_x$ is mainly influenced by κ_{ph} . For Al-doped Mg_2Si , the ratio of κ_{el} to κ_{ph} at 302 K is 8%, and it is 24% at 873 K. For Al-doped $Mg_2Si_{0.9}Sn_{0.1}$ ($y=0.02$), the ratio of κ_{el} to κ_{ph} at 312 K is 21%, and it is 36% at 864 K.

Fig. 7 shows the temperature dependence of the power factor ($P=S^2/\rho$) of Al-doped $Mg_2Si_{1-x}Sn_x$ ($x=0.0-0.1$), compared with those of $Mg_2Si_{1-x}Sn_x$ without Al-doping. The maximum power factor of Al-doped $Mg_2Si_{1-x}Sn_x$ depends on x as well as the Al-doping concentration. As a result that the mobility of Al-doped $Mg_2Si_{1-x}Sn_x$ decreases by the substitution of Sn, the maximum power factor of Al-doped $Mg_2Si_{1-x}Sn_x$ decreases by the substitution of Sn. Al-doped Mg_2Si without Sn substitution shows the maximum power factor is 2.8×10^{-5} W/(cm K²) at 312 K. The maximum power factor of Al-doped Mg_2Si is slightly higher than that of a previous experimental value of 0.15 at% Al-doped Mg_2Si [2.2×10^{-5} W/(cm K²) at 470–560 K] [9], but is lower than that of Sb-doped Mg_2Si [3.4×10^{-5} W/(cm K²) at 476 K for $x=0.005$] [33]. The electrical resistivity at 300 K of Al-doped Mg_2Si in this study is lower than that of the previous reported 0.15 at% Al-doped Mg_2Si and the absolute value of S at ~ 310 K of Al-doped Mg_2Si is slightly higher than that of 0.15 at% Al-doped Mg_2Si . The difference in power factor between Al-doped Mg_2Si and Sb-doped Mg_2Si will be explained by the difference in solubility limit of dopant in Mg_2Si . The electron concentration of Al-doped Mg_2Si (5.3×10^{19} cm⁻³ at 300 K for $x=0.005$) is lower than those of Sb-doped Mg_2Si (7.6×10^{19} cm⁻³ at 300 K for $x=0.005$) and the electron concentration at 300 K is controlled up to 1.5×10^{20} cm⁻³ by Sb-doping.

Fig. 8 shows the temperature dependence of ZT of Al-doped $Mg_2Si_{1-x}Sn_x$ ($x=0.0-0.1$), compared with those of $Mg_2Si_{1-x}Sn_x$ without Al-doping. The maximum values of ZT for $Mg_2Si_{1-x}Sn_x$ without Al-doping show 0.054 at 862 K, 0.13

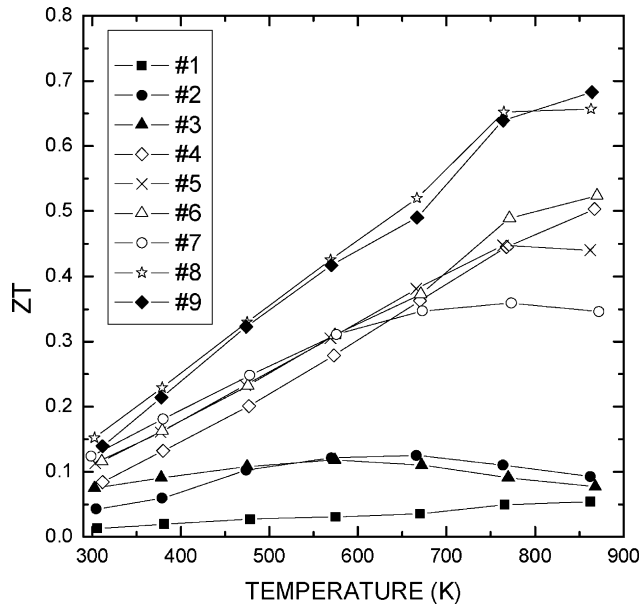


Fig. 8. Dimensionless figure of merit (ZT) of Al-doped $Mg_2Si_{1-x}Sn_x$ ($x=0.0-0.1$), compared with those of $Mg_2Si_{1-x}Sn_x$ without Al-doping.

at 666 K, and 0.12 at 574 K, for $x=0.00, 0.05$, and 0.10 , respectively. On the other hand, the maximum values of ZT for Al-doped $Mg_2Si_{1-x}Sn_x$ show 0.50 at 867 K, 0.52 at 870 K, and 0.68 at 864 K, for $x=0.00, 0.05$, and 0.10 , respectively. Al-doped $Mg_2Si_{0.9}Sn_{0.1}$ shows a highest value of ZT of 0.68 at 864 K, which is 36% larger than that of Al-doped Mg_2Si without Sn substitution. The Z of Al-doped $Mg_2Si_{1-x}Sn_x$ depends on the thermal conductivity as well as the power factor. The power factor of Al-doped $Mg_2Si_{1-x}Sn_x$ depends strongly on its Al-doping concentration. The carrier concentration of Al-doped $Mg_2Si_{1-x}Sn_x$ is controlled up to $5.3 \times 10^{19} \text{ cm}^{-3}$ by Al-doping, but the amount of Sn substitution does not affect the carrier concentration. Therefore, the maximum power factor of Al-doped $Mg_2Si_{1-x}Sn_x$ shows a weak x dependence in the composition range of $0 \leq x \leq 0.1$. However, the thermal conductivity of Al-doped $Mg_2Si_{1-x}Sn_x$ is strongly affected by x . A small amount of Sn substitution ($x \leq 0.1$) plays an important part in reducing the thermal conductivity of Al-doped $Mg_2Si_{1-x}Sn_x$, and a higher ZT has been achieved by the Sn substitution.

4. Conclusions

The thermoelectric properties of Al-doped $Mg_2Si_{1-x}Sn_x$ ($x=0.0-0.1$) [$Mg_2Si_{1-x}Sn_x:Al=1:y$ ($0.00 \leq y \leq 0.02$)] fabricated by spark plasma sintering have been characterized by Hall effect measurements at 300 K and by measurements of electrical resistivity, the Seebeck coefficient, and thermal conductivity between 300 and 900 K. Al-doped $Mg_2Si_{1-x}Sn_x$ samples are n-type in the measured temperature range. By Al-doping, electron concentration is controlled up to $5.3 \times 10^{19} \text{ cm}^{-3}$ in the composition range $0.0 \leq x \leq 0.1$. Al-doped $Mg_2Si_{0.9}Sn_{0.1}$ shows a

maximum value of the figure of merit ZT of 0.68 at 864 K, which is 6 times larger than that of nondoped $Mg_2Si_{0.9}Sn_{0.1}$.

Acknowledgement

This research was partially supported by a grant-in-aid for Young Scientists (B) from the Ministry of Education, Culture, Sports, Science and Technology, no. 18760514, 2007.

References

- [1] R.J. LaBatz, D.R. Mason, D.F. O'Kane, J. Electrochem. Soc. 110 (1963) 127.
- [2] E.N. Nikitin, V.G. Bazanov, V.I. Tarasov, Sov. Phys. Solid State 3 (1962) 2648.
- [3] Y. Noda, H. Kon, Y. Furukawa, N. Otsuka, I.A. Nishida, K. Masumoto, Mater. Trans. JIM 33 (1992) 845.
- [4] Y. Noda, H. Kon, Y. Furukawa, N. Otsuka, I.A. Nishida, K. Masumoto, Mater. Trans. JIM 33 (1992) 851.
- [5] V.K. Zaitsev, M.I. Fedorov, E.A. Gurieva, I.S. Eremin, P.P. Kondtantinov, A.Yu. Samunin, M.V. Vedernikov, Phys. Rev. B 74 (2006) 045207.
- [6] R.G. Morris, R.D. Redin, G.C. Danielson, Phys. Rev. 109 (1958) 1909.
- [7] R.D. Redin, R.G. Morris, G.C. Danielson, Phys. Rev. 109 (1958) 1916.
- [8] M.W. Heller, G.C. Danielson, J. Phys. Chem. Solids 23 (1962) 601.
- [9] M. Umamoto, Y. Shirai, K. Tsuchiya, Proceedings of the 4th Pacific Rim International Conference on Advanced Materials and Processing (PRICM4), 2001, p. 2145.
- [10] J. Tani, H. Kido, Physica B 364 (2005) 218.
- [11] J. Tani, H. Kido, Jpn. J. Appl. Phys. Part 1 46 (2007) 3309.
- [12] C.B. Vining, in: D.M. Rowe (Ed.), CRC Handbook of Thermoelectrics, CRC Press, Boca Raton, 1995, p. 277.
- [13] V.K. Zaitsev, M.I. Fedorov, I.S. Eremin, E.A. Gurieva, in: D.M. Rowe (Ed.), Thermoelectrics Handbook Macro to Nano, CRC Press, Boca Raton, 2006, Chapter 29.
- [14] T. Kajikawa, K. Shida, S. Sugihara, M. Ohmori, T. Hirai, Proceedings of 16th International Conference on Thermoelectrics (ICT'97), 1997, p. 275.
- [15] M.W. Chase Jr., JANAF Thermochemical Table J. Phys. Chem. Ref. Data 14 (Suppl. 1) (1985) 1495.
- [16] M.D. Segall, P.J.D. Lindan, M.J. Probert, C.J. Pickard, P.J. Hasnip, S.J. Clark, M.C. Payne, J. Phys. Condens. Matter 14 (2002) 2717.
- [17] H.J. Monkhorst, J.D. Pack, Phys. Rev. B 13 (1976) 5188.
- [18] D. Vanderbilt, Phys. Rev. B 41 (1990) 7892.
- [19] J.G. Barlock, L.F. Mondolfo, Z. Metallkd. 66 (1975) 605.
- [20] G. Busch, U. Winkler, Helv. Phys. Acta 26 (1953) 359.
- [21] G. Busch, U. Winkler, Physica 20 (1954) 1067.
- [22] V.K. Zaitsev, E.N. Nikitin, E.N. Tkalenko, Sov. Phys. Solid State 11 (1969) 3000.
- [23] Y. Imai, A. Watanabe, M. Mukaida, J. Alloys Compd. 358 (2003) 257.
- [24] S.B. Zhang, J.E. Northrup, Phys. Rev. Lett. 67 (1991) 2339.
- [25] D.B. Laks, C.G. Van de Walle, G.F. Neumark, P.E. Blöchl, S.T. Pantelides, Phys. Rev. B 45 (1992) 10965.
- [26] C.G. Van de Walle, D.B. Laks, G.F. Neumark, S.T. Pantelides, Phys. Rev. B 47 (1993) 9425.
- [27] See, for example A.F. Ioffe, Semiconductor Thermoelements and Thermoelectric Cooling, Infosearch, London, 1957.
- [28] J. McDougall, E.C. Stoner, Philos. Trans. R. Soc. London Ser. A 237 (1938) 67.
- [29] P. Rhoads, Proc. R. Soc. London Ser. A 204 (1950) 396.
- [30] A.C. Beer, M.N. Chase, P.F. Choquard, Helv. Phys. Acta 28 (1955) 529.
- [31] R.B. Dingle, Appl. Sci. Res. B 6 (1957) 225.
- [32] See, for example N.W. Ashcroft, N.D. Mermin, Solid State Physics, Holt, Rinehart, Winston, New York, 1976 (and references therein, p. 20).
- [33] J. Tani, H. Kido, Intermetallics 15 (2007) 1202.